

CONSTRUCTIVE APPROXIMATION OF RANDOM PROCESS VIA STOCHASTIC INTERPOLATION NEURAL NETWORK OPERATORS

Sachin Saini Uaday Singh

Department of Mathematics
Indian Institute of Technology Roorkee
Roorkee, 247667, India

sachin_saini@ma.iitr.ac.in, uaday.singh@ma.iitr.ac.in

January 1, 2026

ABSTRACT

In this paper, we construct a class of stochastic interpolation neural network operators (SINNOs) with random coefficients activated by sigmoidal functions. We establish their boundedness, interpolation accuracy, and approximation capabilities in the mean square sense, in probability, as well as pathwise within the space of second-order stochastic (random) processes $L^2(\Omega, \mathcal{F}, \mathbb{P})$. Additionally, we provide quantitative error estimates using the modulus of continuity of the processes. These results highlight the effectiveness of SINNOs for approximating stochastic processes with potential applications in COVID-19 case prediction.

Keywords Sigmoidal function, Neural network operators, Stochastic interpolation, Mean square approximation, Uniform approximation.

MSC Classification: 41A05, 41A25, 41A28, 47A58, 60H35, 82C32.

1 Introduction

In recent years, artificial neural networks have successfully advanced in function approximation, pattern recognition, and machine learning. Research by Cybenko [1] and Funahashi [2] demonstrated that single-layer feed-forward neural networks (FNNs) can approximate continuous deterministic functions with arbitrary precision, provided they have a sufficient number of hidden neurons. These networks are now widely applied in computer science, biology, mathematics, physics, and engineering. Typically, an FNNs with one hidden layer can be mathematically expressed as

$$\mathbf{N}_n(\mathbf{t}) = \sum_{k=0}^n c_k \eta(\mathbf{a}_k \cdot \mathbf{t} + b_k), \quad (1)$$

where $\mathbf{t} = (t_1, t_2, \dots, t_d)$, $\mathbf{a}_k \in \mathbb{R}^d$, $c_k, b_k \in \mathbb{R}$, and η denotes the activation function.

The theory of *neural network operators* (NNOs) provides a constructive framework for approximating functions using FNNs. Cardaliaguet and Euvrard [3] were the first to distinguish two types of NNOs: bell-shaped and squashing-type. These operators offer explicit formulations for approximating a function and its derivatives through a single-hidden-layer neural network using suitable activation functions. Later, Anastassiou [4, 5] investigated the convergence rates of such operators and further extended the analysis for various activation functions [6, 7, 8, 9, 10, 11].

Deterministic interpolation-type NNOs activated by the ramp function were first defined by Costarelli [12, 13] as

$$F_n(f, t) = \frac{\sum_{k=0}^n f(t_k) \varphi_R\left(\frac{n(t-t_k)}{b-a}\right)}{\sum_{j=0}^n \varphi_R\left(\frac{n(t-t_j)}{b-a}\right)}, \quad t \in [a, b], \quad (2)$$

where the nodes t_k are uniformly spaced as $t_k = a + k\delta$ with $\delta = \frac{b-a}{n}$. Subsequently, Qian et al. [14] generalized this construction for a broader class of activation functions η , defining

$$S_n(f, t) = \sum_{k=0}^n f(t_k) \varphi_{\mathcal{A}(m)}\left(\frac{2m}{\delta}(t - t_k)\right), \quad t \in [a, b], \quad (3)$$

where $\varphi_{\mathcal{A}(m)}(t) = \eta(t + m) - \eta(t - m)$. Further developments include multivariate extensions [15, 16, 17] and irregular grid formulations [18, 19, 20] and in fuzzy settings extension [21].

Despite their theoretical richness, most NNOs remain deterministic. However, many real-world signals and physical processes are inherently stochastic, with uncertainty arising from environmental noise or intrinsic randomness rather than measurement error. To address such cases, neural networks must be capable of learning mappings involving random functions and probabilistic dependencies. This perspective has motivated the development of *stochastic neural networks* (SNNs), such as Boltzmann-type models introduced by Amari et al. [22] and recurrent stochastic networks explored by Zhao et al. [23]. Belli et al. [24] later established that SNNs can approximate stochastic processes in the mean square sense. Makovoz [25] and Anastassiou [26, 27, 28, 29] subsequently extended NNOs to random and time-separating processes.

Recent research trends also emphasize stochasticity and uncertainty quantification in neural network models. For instance, Gal and Ghahramani's stochastic dropout framework has inspired further exploration of test-time uncertainty modeling through random weight injection [30], while Durrmeyer-type deep neural networks [31] established a rigorous connection between classical integral operators and neural architectures. Similarly, neural approaches have been utilized for modeling stochastic systems with jump dynamics [32], and fuzzy-stochastic hybrids have been developed for uncertainty-aware process modeling [33]. From a theoretical standpoint, the expressive power of stochastic neural architectures has been analyzed using refined Kolmogorov complexity measures [34], providing formal insight into their representational capabilities.

Motivated by these developments, in this paper we introduce a new class of *stochastic interpolation neural network operators* (SINNOs) which generalize traditional deterministic NNOs to the stochastic setting, providing an operator-based framework for approximating second-order processes $X_t(\omega) \in L^2(\Omega, \mathcal{F}, \mathbb{P})$. The proposed SINNOs integrate stochasticity at the operator level through random coefficients $X_{t_k}(\omega)$ while preserving the analytical and structural properties of deterministic interpolation operators. From an application standpoint, these operators effectively handle real-world signals, as demonstrated through their implementation on both simulated stochastic processes and real COVID-19 case data.

2 Preliminaries

Let $(\Omega, \mathcal{F}, \mathbb{P})$ be a probability space and let $\mathcal{T} = [0, T]$. A *stochastic process* is a family $(X_t)_{t \in \mathcal{T}}$ of random variables $X_t : (\Omega, \mathcal{F}) \rightarrow \mathbb{R}$. We say that X_t is *square-integrable* if $X_t \in L^2(\Omega, \mathcal{F}, \mathbb{P})$, i.e.,

$$\mathbb{E}[|X_t|] < \infty, \quad \mathbb{E}[|X_t|^2] < \infty.$$

Throughout, we assume that for each $t \in \mathcal{T}$, $X_t \in L^2(\Omega, \mathcal{F}, \mathbb{P})$. Here, Ω denotes the sample space, \mathcal{F} is a σ -algebra of events, and \mathbb{P} is a probability measure on \mathcal{F} . The symbol $\mathbb{E}(\cdot)$ denotes the mathematical expectation. See [35] for foundational details on stochastic processes.

Definition 2.1. A measurable function $\eta : \mathbb{R} \rightarrow \mathbb{R}$ is called a *sigmoidal function* if

$$\lim_{t \rightarrow -\infty} \eta(t) = 0 \quad \text{and} \quad \lim_{t \rightarrow +\infty} \eta(t) = 1.$$

Definition 2.2. Let $m > 0$ be fixed. A sigmoidal function η is said to belong to the class $\mathcal{A}(m)$ if the following conditions hold:

\mathcal{A}_1 : $\eta(t)$ is non-decreasing;

\mathcal{A}_2 : $\eta(t) = 1$ for $t \geq m$ and $\eta(t) = 0$ for $t \leq -m$.

For $\eta \in \mathcal{A}(m)$, we define the corresponding *activation function* by

$$\varphi_{\mathcal{A}(m)}(t) = \eta(t + m) - \eta(t - m), \quad t \in \mathbb{R}.$$

Remark 2.3. Some examples of sigmoidal functions satisfying the above conditions are as follows:

(i) **Ramp function:**

$$\eta_R(t) = \begin{cases} 0, & t \leq -\frac{1}{2}, \\ t + \frac{1}{2}, & -\frac{1}{2} < t < \frac{1}{2}, \\ 1, & t \geq \frac{1}{2}. \end{cases}$$

It is easy to verify that $\eta_R \in \mathcal{A}(1/2)$.

(ii) **Sigmoidal functions generated by central B -splines:** The B -spline of order r is defined by

$$M_r(t) = \frac{1}{(r-1)!} \sum_{j=0}^r (-1)^j \binom{r}{j} \left(\frac{r}{2} + t - j\right)_+^{r-1},$$

where $(t)_+ := \max\{t, 0\}$ denotes the positive part of $t \in \mathbb{R}$. The associated sigmoidal function is defined by

$$\eta_{M(r)}(t) := \int_{-\infty}^t M_r(y) dy, \quad t \in \mathbb{R}.$$

Since $\text{supp}(M_r) \subset [-r/2, r/2]$ and $M_r \geq 0$, it follows that $\eta_{M(r)}(t) = 0$ for $t \leq -r/2$ and $\eta_{M(r)}(t) = 1$ for $t \geq r/2$. Therefore, $\eta_{M(r)} \in \mathcal{A}(r/2)$.

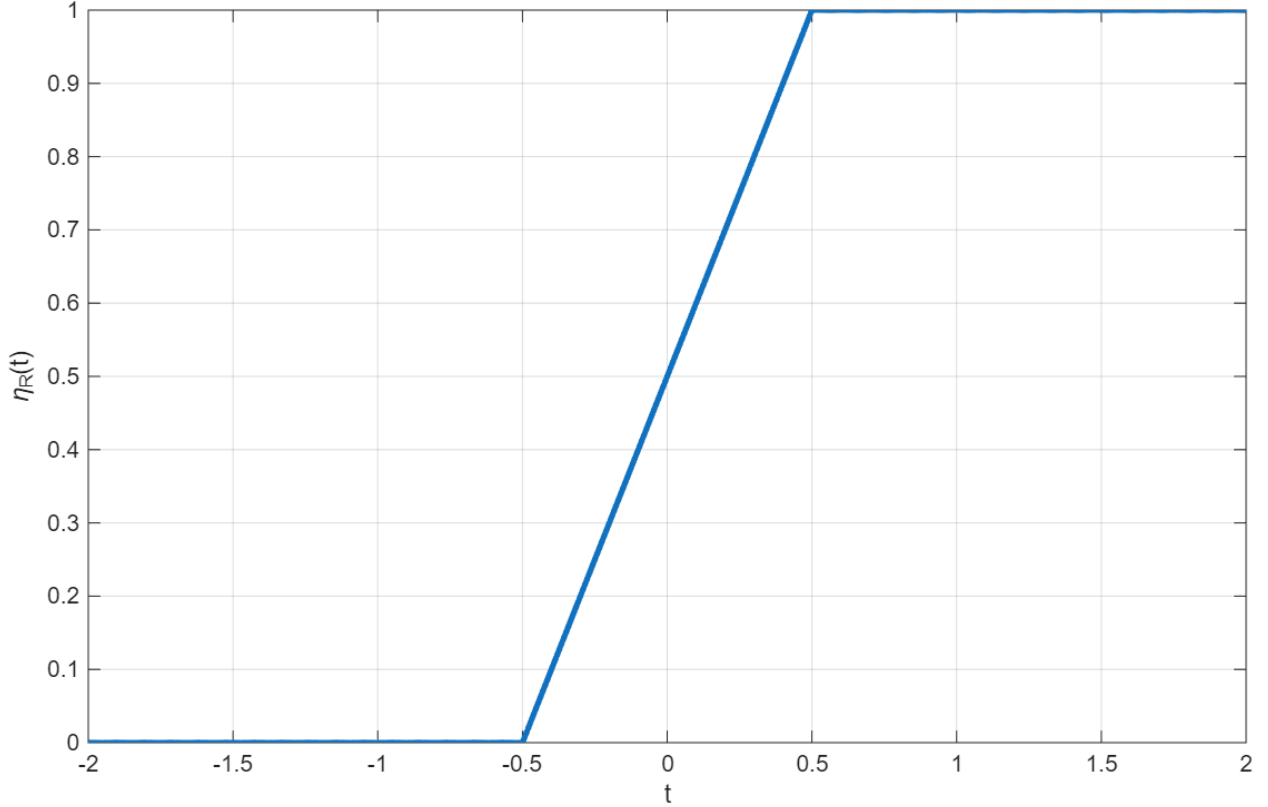


Figure 1: Sigmoidal ramp function η_R .

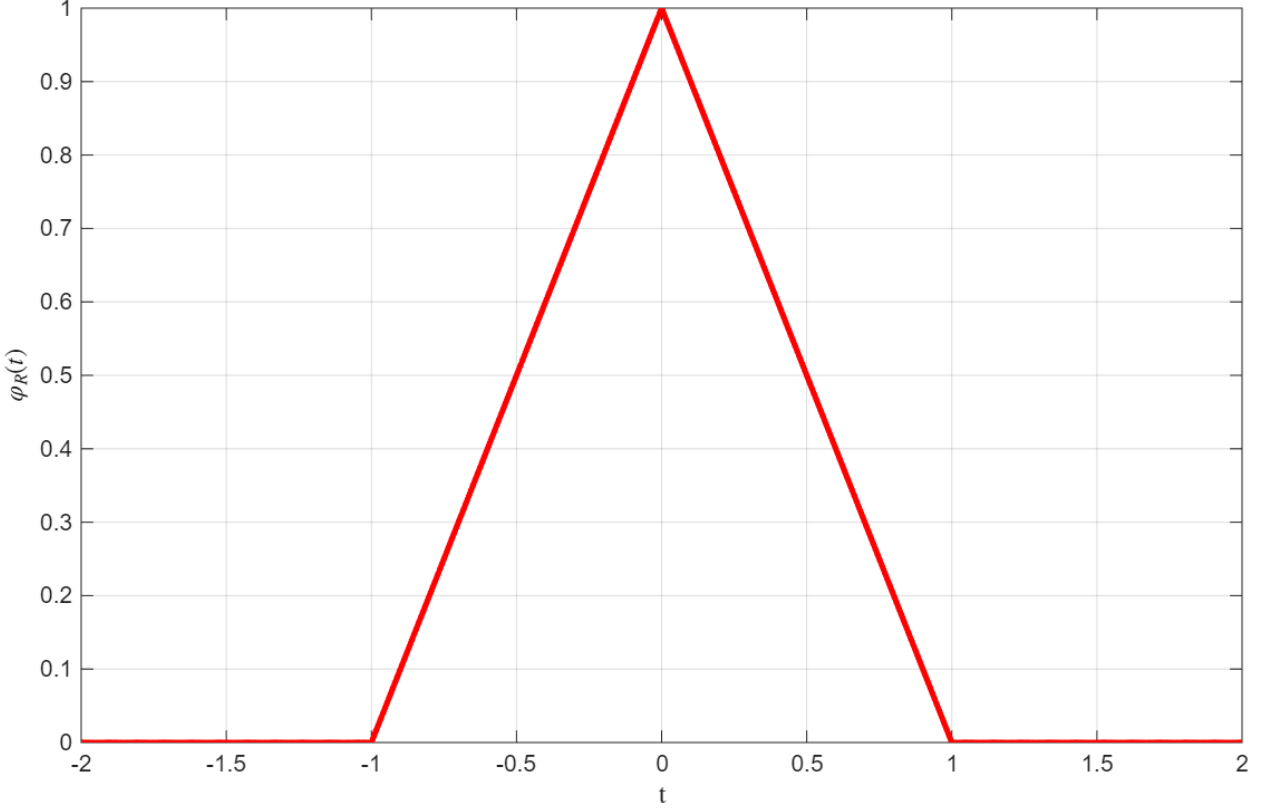


Figure 2: Activation function φ_R corresponding to the ramp function η_R .

Definition 2.4 (Discrete absolute moments of order α). For $\alpha \geq 0$, the discrete absolute moments of order α for the activation function $\varphi_{\mathcal{A}(m)}$ are defined by

$$\mathcal{M}_\alpha(\varphi_{\mathcal{A}(m)}) = \sup_{t \in \mathbb{R}} \sum_{k \in \mathbb{Z}} |\varphi_{\mathcal{A}(m)}(t - t_k)| |t - t_k|^\alpha.$$

We summarize below some useful properties of $\varphi_{\mathcal{A}(m)}(t)$. See [14, 36] for detailed proofs.

Lemma 2.5. *If $\eta \in \mathcal{A}(m)$, then the activation function $\varphi_{\mathcal{A}(m)}$ satisfies:*

- (M1) $\varphi_{\mathcal{A}(m)}(t) \geq 0$ for all $t \in \mathbb{R}$;
- (M2) $\varphi_{\mathcal{A}(m)}(t)$ is non-decreasing for $t < 0$ and non-increasing for $t \geq 0$;
- (M3) $\text{supp}(\varphi_{\mathcal{A}(m)}) \subseteq [-2m, 2m]$;
- (M4) $\varphi_{\mathcal{A}(m)}(t) + \varphi_{\mathcal{A}(m)}(t - 2m) = 1$ for $t \in [0, 2m]$;
- (M5) $\mathcal{M}_0(\varphi_{\mathcal{A}(m)}) < \infty$.

Lemma 2.6 (M5). *Let $\eta \in \mathcal{A}(m)$. For every $\alpha \geq 0$, the discrete absolute moment $\mathcal{M}_\alpha(\varphi_{\mathcal{A}(m)})$ is finite and satisfies*

$$\mathcal{M}_\alpha(\varphi_{\mathcal{A}(m)}) \leq (2m)^\alpha (\lfloor 4m \rfloor + 2).$$

In particular, $\mathcal{M}_0(\varphi_{\mathcal{A}(m)}) \leq \lfloor 4m \rfloor + 2 < \infty$, which verifies (M5).

Proof. By (M3), $\text{supp}(\varphi_{\mathcal{A}(m)}) \subseteq [-2m, 2m]$. So, for any fixed $t \in \mathbb{R}$,

$$\varphi_{\mathcal{A}(m)}(t - k) \neq 0 \implies |t - k| \leq 2m.$$

Thus, only integers k in the interval $[t - 2m, t + 2m]$ contribute to the sum. The number of such integers is at most $\lfloor 4m \rfloor + 2$. Using $0 \leq \varphi_{\mathcal{A}(m)}(t) \leq 1$, we have

$$\begin{aligned} \sum_{k \in \mathbb{Z}} |\varphi_{\mathcal{A}(m)}(t - k)| |t - k|^\alpha &\leq \sum_{\substack{k \in \mathbb{Z} \\ |t - k| \leq 2m}} |t - k|^\alpha \\ &\leq (2m)^\alpha (\lfloor 4m \rfloor + 2). \end{aligned}$$

Taking the supremum over $t \in \mathbb{R}$ yields the stated bound. \square

Definition 2.7 (Mean Square Convergence). Let $\{X_n(t, \omega)\}_{n \in \mathbb{N}}$ be a sequence of stochastic processes and let $X(t, \omega)$ be another stochastic process defined on the same probability space $(\Omega, \mathcal{F}, \mathbb{P})$. We say that X_n converges to X in the mean square sense (or in L^2) if, for every fixed t in the domain of definition,

$$\lim_{n \rightarrow \infty} \mathbb{E}[|X_n(t, \omega) - X(t, \omega)|^2] = 0.$$

Equivalently, $X_n \rightarrow X$ in mean square if and only if

$$\|X_n(t, \cdot) - X(t, \cdot)\|_{L^2(\Omega)} := (\mathbb{E}[|X_n(t, \omega) - X(t, \omega)|^2])^{1/2} \rightarrow 0 \quad \text{as } n \rightarrow \infty.$$

3 Stochastic Interpolation Neural Network Operators

In this section, we introduce the SINNOs with random coefficients. We then establish their well-definedness and boundedness, followed by deriving their approximation properties in the mean-square sense, in probability and along individual sample paths.

Definition 3.1. Let $(X_t)_{t \in \mathcal{T}}$ be a stochastic process defined on the probability space $(\Omega, \mathcal{F}, \mathbb{P})$, and let $\eta \in \mathcal{A}(m)$. The corresponding *stochastic interpolation neural network operators* (SINNOs) with random coefficients activated by $\varphi_{\mathcal{A}(m)}$ are defined by

$$\mathcal{S}_n(X_t, t) := \sum_{k=0}^n X_{t_k}(\omega) \varphi_{\mathcal{A}(m)}\left(\frac{2m}{\delta}(t - t_k)\right), \quad t \in \mathcal{T}, \omega \in \Omega, \quad (4)$$

where the nodes $\{t_k\}_{k=0}^n$ are uniformly spaced points in $\mathcal{T} = [0, T]$ given by

$$t_k = k\delta, \quad k = 0, 1, \dots, n,$$

and $\delta = \frac{T}{n}$ denotes the uniform step size.

The operator $\mathcal{S}_n(X_t, t)$ acts as a stochastic interpolant of the process $X_t(\omega)$, where each realization of the random coefficients $X_{t_k}(\omega)$ is modulated by the compactly supported activation function $\varphi_{\mathcal{A}(m)}$. The structure of the above-defined SINNOs is illustrated in Figure 3.

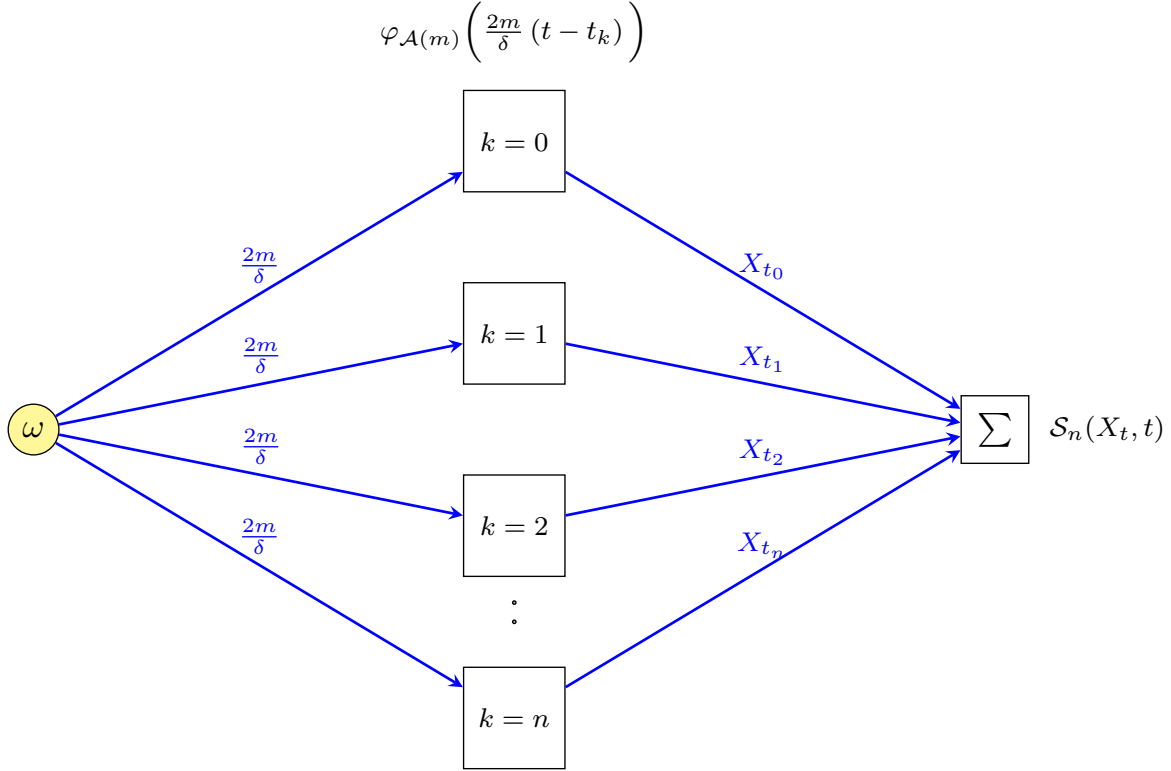


Figure 3: Structure of the above-defined SINNOs $\mathcal{S}_n(X_t, t)$.

Firstly, we show that the operator $\mathcal{S}_n(X_t, t)$ is well-defined and bounded in the mean-square sense within the space $L^2(\Omega, \mathcal{F}, \mathbb{P})$.

Theorem 3.2 (Mean-square boundedness of SINNOs). *Let $(X_t)_{t \in \mathcal{T}}$ be a stochastic process such that $X_t \in L^2(\Omega, \mathcal{F}, \mathbb{P})$ for each $t \in \mathcal{T}$, and let $\varphi_{\mathcal{A}(m)}$ be the activation function corresponding to a sigmoidal function $\eta \in \mathcal{A}(m)$. Then, for every $t \in \mathcal{T}$,*

$$\mathbb{E} \left[|\mathcal{S}_n(X_t, t)|^2 \right] \leq \mathcal{M}_0^2(\varphi_{\mathcal{A}(m)}) \sup_{s \in \mathcal{T}} \mathbb{E}[|X_s|^2], \quad (5)$$

where $\mathcal{M}_0(\varphi_{\mathcal{A}(m)})$ denotes the discrete absolute moment of order zero (see Lemma 2.6).

Proof. From Definition 3.1, we have

$$\mathcal{S}_n(X_t, t) = \sum_{k=0}^n X_{t_k}(\omega) \varphi_{\mathcal{A}(m)} \left(\frac{2m}{\delta} (t - t_k) \right).$$

Since each $X_{t_k} \in L^2(\Omega, \mathcal{F}, \mathbb{P})$ and $\varphi_{\mathcal{A}(m)}$ is bounded, $\mathcal{S}_n(X_t, t)$ is a finite linear combination of L^2 random variables and hence belongs to $L^2(\Omega, \mathcal{F}, \mathbb{P})$.

Expanding the square and applying linearity of expectation gives

$$\begin{aligned} \mathbb{E} \left[|\mathcal{S}_n(X_t, t)|^2 \right] &= \mathbb{E} \left[\sum_{k=0}^n \sum_{j=0}^n X_{t_k}(\omega) X_{t_j}(\omega) \varphi_{\mathcal{A}(m)} \left(\frac{2m}{\delta} (t - t_k) \right) \varphi_{\mathcal{A}(m)} \left(\frac{2m}{\delta} (t - t_j) \right) \right] \\ &= \sum_{k=0}^n \sum_{j=0}^n \mathbb{E}[X_{t_k} X_{t_j}] \varphi_{\mathcal{A}(m)} \left(\frac{2m}{\delta} (t - t_k) \right) \varphi_{\mathcal{A}(m)} \left(\frac{2m}{\delta} (t - t_j) \right). \end{aligned}$$

Using the Cauchy-Schwarz inequality,

$$|\mathbb{E}[X_{t_k} X_{t_j}]| \leq (\mathbb{E}[|X_{t_k}|^2])^{1/2} (\mathbb{E}[|X_{t_j}|^2])^{1/2} \leq \sup_{s \in \mathcal{T}} \mathbb{E}[|X_s|^2].$$

Hence,

$$\mathbb{E}[|\mathcal{S}_n(X_t, t)|^2] \leq \sup_{s \in \mathcal{T}} \mathbb{E}[|X_s|^2] \left(\sum_{k=0}^n |\varphi_{\mathcal{A}(m)}\left(\frac{2m}{\delta}(t - t_k)\right)| \right)^2.$$

By Lemma 2.6 (for $\alpha = 0$),

$$\sup_{t \in \mathbb{R}} \sum_{k \in \mathbb{Z}} |\varphi_{\mathcal{A}(m)}(t - t_k)| \leq \mathcal{M}_0(\varphi_{\mathcal{A}(m)}),$$

which yields the desired bound. \square

We will now explore the interpolation and approximation properties of the sequence of operators, $\mathcal{S}_n(X_t, t)$ defined in (3.1) in the mean square sense.

Theorem 3.3. *Let $(X_t)_{t \in \mathcal{T}}$ be such that $X_t \in L^2(\Omega, \mathcal{F}, \mathbb{P})$ for every t , and let $\eta \in \mathcal{A}(m)$. Then for each node $t_i = i\delta$ ($i = 0, 1, \dots, n$),*

$$\mathbb{E}[|\mathcal{S}_n(X_t, t_i) - X_{t_i}|^2] = 0.$$

Proof. Fix a node t_i . Write the interpolation error at t_i , as a random variable

$$\mathcal{E}(\omega) := \mathcal{S}_n(X_t, t_i) - X_{t_i}(\omega) = \sum_{k=0}^n (X_{t_k}(\omega) - X_{t_i}(\omega)) \varphi_{\mathcal{A}(m)}\left(\frac{2m}{\delta}(t_i - t_k)\right).$$

Because each $\varphi_{\mathcal{A}(m)}(\cdot)$ is deterministic, we expand the mean square of \mathcal{E} and shift the deterministic terms outside the expectation:

$$\begin{aligned} \mathbb{E}[|\mathcal{E}|^2] &= \mathbb{E}\left[\left(\sum_{k=0}^n (X_{t_k} - X_{t_i}) \varphi_k\right) \left(\sum_{j=0}^n (X_{t_j} - X_{t_i}) \varphi_j\right)\right] \\ &= \sum_{k=0}^n \sum_{j=0}^n \varphi_k \varphi_j \mathbb{E}[(X_{t_k} - X_{t_i})(X_{t_j} - X_{t_i})], \end{aligned} \quad (6)$$

where we abbreviated $\varphi_k := \varphi_{\mathcal{A}(m)}\left(\frac{2m}{\delta}(t_i - t_k)\right)$. Now using the support property (M3), for any $k \neq i$, we have

$$\left| \frac{2m}{\delta}(t_i - t_k) \right| = 2m|i - k| \geq 2m,$$

so $\varphi_k = 0$ for all $k \neq i$. Consequently every term in (6) with $k \neq i$ or $j \neq i$ vanishes, leaving only the $(k, j) = (i, i)$ term:

$$\mathbb{E}[|\mathcal{E}|^2] = \varphi_i^2 \mathbb{E}[(X_{t_i} - X_{t_i})^2] = \varphi_i^2 \cdot 0 = 0.$$

Therefore, $\mathbb{E}[|\mathcal{S}_n(X_t, t_i) - X_{t_i}|^2] = 0$, as required. \square

Theorem 3.4. *If $X_t(\omega) = 1$ for all $t \in \mathcal{T}$ and $\omega \in \Omega$, then*

$$\mathbb{E}[|\mathcal{S}_n(1, t) - 1|^2] = 0, \quad \forall t \in \mathcal{T}.$$

Proof. Fix $t \in \mathcal{T}$. Since $\varphi_{\mathcal{A}(m)}$ is deterministic (i.e. independent of ω), the SINNOs applied to the constant function reduces to the deterministic finite sum

$$\mathcal{S}_n(1, t) = \sum_{k=0}^n \varphi_{\mathcal{A}(m)}\left(\frac{2m}{\delta}(t - t_k)\right).$$

Hence, the mean-square error is just the square of a deterministic number:

$$\mathbb{E}[|\mathcal{S}_n(1, t) - 1|^2] = \left(\sum_{k=0}^n \varphi_{\mathcal{A}(m)}\left(\frac{2m}{\delta}(t - t_k)\right) - 1 \right)^2.$$

If $t \in [t_i, t_{i+1}]$, then by (M3) only the terms with $k = i$ and $k = i + 1$ can be nonzero. By the partition-of-unity property (M4) which proves the theorem. \square

We will now examine the quantitative estimates for the sequence of operators $\mathcal{S}_n(X_t, t)$ defined in (3.1) in the space $L^2(\Omega, \mathcal{F}, \mathbb{P})$ and measure the rate of approximation in terms of modulus of continuity defined below.

Let $X_t(\omega) \in L^2(\Omega, \mathcal{F}, \mathbb{P})$. For $h > 0$, the function

$$\mathcal{W}(X_t, h) = \max \{ \mathbb{E}|X_t(\omega) - X_s(\omega)|^2 : t, s \in \mathcal{T}, |s - t| \leq h \},$$

is known as the modulus of continuity of $X_t(\omega)$.

The following theorem outlines several key properties of the modulus of continuity defined above.

Theorem 3.5. *Let $X_t(\omega) \in L^2(\Omega, \mathcal{F}, \mathbb{P})$. Then*

- (i) $\mathcal{W}(X_t, h)$ is non-decreasing in h ;
- (ii) If $X_t(\omega)$ is mean square continuous, then $\mathcal{W}(X_t, h)$ is continuous in h , and $\mathcal{W}(X_t, h) \rightarrow 0$ as $h \rightarrow 0_+$;
- (iii) If $X_t(\omega)$ is a stochastic process with

$$\mathbb{E}|X_t(\omega) - X_s(\omega)|^2 \leq C|t - s|^\alpha$$

for some constant $C > 0$ and exponent $0 < \alpha \leq 1$, then the modulus of continuity $\mathcal{W}(X_t, h)$ is bounded and

$$\mathcal{W}(X_t, h) \leq Ch^\alpha;$$

- (iv) Let $X_t(\omega)$ and $Y_t(\omega)$ be two independent stochastic processes. Then

$$\mathcal{W}(X_t + Y_t, h) \leq \mathcal{W}(X_t, h) + \mathcal{W}(Y_t, h);$$

- (v) Let $X_t(\omega)$ and $Y_t(\omega)$ be two dependent stochastic processes. Then

$$\mathcal{W}(X_t + Y_t, h) \leq \mathcal{W}(X_t, h) + \mathcal{W}(Y_t, h) + 2\sqrt{\mathcal{W}(X_t, h)\mathcal{W}(Y_t, h)}.$$

Proof. (i) It is obvious that, by the definition of $\mathcal{W}(X_t, h)$, it takes the supremum over all pairs t, s such that $|t - s| \leq h$. Therefore, increasing h only adds more terms to the maximization set, ensuring that $\mathcal{W}(X_t, h)$ does not decrease.

- (ii) By the definition of $\mathcal{W}(X_t, h)$, we have

$$\mathcal{W}(X_t, h) = \max \{ \mathbb{E}|X_t(\omega) - X_s(\omega)|^2 : t, s \in \mathcal{T}, |s - t| \leq h \}.$$

Since $X_t(\omega)$ is mean-square continuous, it follows that for any $\epsilon > 0$, there exists some $h_0 > 0$ such that

$$\mathbb{E}|X_t(\omega) - X_s(\omega)|^2 < \epsilon \quad \text{whenever } |t - s| < h_0.$$

Taking the supremum over all pairs (t, s) such that $|s - t| \leq h$, we obtain

$$\mathcal{W}(X_t, h) \rightarrow 0 \quad \text{as } h \rightarrow 0.$$

Thus, the modulus of continuity $\mathcal{W}(X_t, h)$ is right-continuous at $h = 0$.

- (iii) By the definition of the modulus of continuity, we have

$$\mathcal{W}(X_t, h) = \max \{ \mathbb{E}|X_t(\omega) - X_s(\omega)|^2 : |s - t| \leq h \}.$$

Given that $\mathbb{E}|X_t(\omega) - X_s(\omega)|^2 \leq C|t - s|^\alpha$, it follows that

$$\mathbb{E}|X_t(\omega) - X_s(\omega)|^2 \leq Ch^\alpha \quad \text{for all } t, s \in \mathcal{T}, |s - t| \leq h.$$

Taking the supremum over all such pairs (t, s) , we get,

$$\mathcal{W}(X_t, h) \leq Ch^\alpha.$$

- (iv) For two independent processes $X_t(\omega)$ and $Y_t(\omega)$, we have

$$\mathbb{E}|X_t(\omega) + Y_t(\omega) - (X_s(\omega) + Y_s(\omega))|^2 = \mathbb{E}|X_t(\omega) - X_s(\omega)|^2 + \mathbb{E}|Y_t(\omega) - Y_s(\omega)|^2.$$

Thus, the maximum of the sum on the RHS over $|t - s| \leq h$ will satisfy

$$\mathcal{W}(X_t + Y_t, h) = \max \{ \mathbb{E}|X_t(\omega) - X_s(\omega)|^2 + \mathbb{E}|Y_t(\omega) - Y_s(\omega)|^2 : |t - s| \leq h \}.$$

This implies

$$\mathcal{W}(X_t + Y_t, h) \leq \mathcal{W}(X_t, h) + \mathcal{W}(Y_t, h).$$

(v) For dependent processes, we use the triangle inequality

$$\begin{aligned} \mathbb{E}|X_t(\omega) + Y_t(\omega) - (X_s(\omega) + Y_s(\omega))|^2 &\leq \mathbb{E}|X_t(\omega) - X_s(\omega)|^2 \\ &\quad + \mathbb{E}|Y_t(\omega) - Y_s(\omega)|^2 \\ &\quad + 2\sqrt{\mathbb{E}|X_t(\omega) - X_s(\omega)|^2 \mathbb{E}|Y_t(\omega) - Y_s(\omega)|^2}. \end{aligned}$$

Taking the supremum over $|t - s| \leq h$, we get

$$\mathcal{W}(X_t + Y_t, h) \leq \mathcal{W}(X_t, h) + \mathcal{W}(Y_t, h) + 2\sqrt{\mathcal{W}(X_t, h)\mathcal{W}(Y_t, h)}.$$

□

Theorem 3.6. Let $X_t(\omega) \in L^2(\Omega, \mathcal{F}, \mathbb{P})$ for every $t \in \mathcal{T}$, and let $\eta \in \mathcal{A}(m)$. For $\delta = T/n$ the SINNOs $\mathcal{S}_n(X_t, t)$ defined in (3.1) satisfies

$$\mathbb{E}[|\mathcal{S}_n(X_t, t) - X_t|^2] \leq \mathcal{W}(X_t, \delta), \text{ for every } t \in \mathcal{T}.$$

Consequently, if X_t is mean-square continuous, then for each fixed t , $\mathcal{S}_n(X_t, t) \xrightarrow{L^2} X_t$ as $n \rightarrow \infty$. Moreover, the convergence is uniform in t ; i.e.,

$$\sup_{t \in \mathcal{T}} \mathbb{E}[|\mathcal{S}_n(X_t, t) - X_t|^2] \leq \mathcal{W}(X_t, \delta) \rightarrow 0, \text{ as } n \rightarrow \infty.$$

Proof. Fix $t \in \mathcal{T}$ and let $t \in [t_i, t_{i+1}]$ for some $i \in \{0, \dots, n-1\}$. By property (M3) of Lemma 2.5 only the two nearest nodes contribute to the sum, so

$$\mathcal{S}_n(X_t, t) = X_{t_i} \varphi\left(\frac{2m}{\delta}(t - t_i)\right) + X_{t_{i+1}} \varphi\left(\frac{2m}{\delta}(t - t_{i+1})\right).$$

Using (M4), we have the partition of unity as

$$\varphi_{\mathcal{A}(m)}\left(\frac{2m}{\delta}(t - t_i)\right) + \varphi_{\mathcal{A}(m)}\left(\frac{2m}{\delta}(t - t_{i+1})\right) = 1. \quad (7)$$

Thus, we rewrite the approximation error as under.

$$\begin{aligned} \mathbb{E}|\mathcal{S}_n(X_t, t) - X_t(\omega)|^2 &= \mathbb{E}\left|\sum_{k=0}^n X_{t_k}(\omega) \varphi_{\mathcal{A}(m)}\left(\frac{2m}{\delta}(t - t_k)\right) - X_t(\omega)\right|^2 \\ &= \mathbb{E}\left|X_{t_i}(\omega) \varphi_{\mathcal{A}(m)}\left(\frac{2m}{\delta}(t - t_i)\right)\right. \\ &\quad \left.+ X_{t_{i+1}}(\omega) \varphi_{\mathcal{A}(m)}\left(\frac{2m}{\delta}(t - t_{i+1})\right) - X_t(\omega)\right|^2 \\ &= \mathbb{E}\left|\left(X_{t_i}(\omega) - X_t(\omega)\right) \varphi_{\mathcal{A}(m)}\left(\frac{2m}{\delta}(t - t_i)\right)\right. \\ &\quad \left.+ \left(X_{t_{i+1}}(\omega) - X_t(\omega)\right) \varphi_{\mathcal{A}(m)}\left(\frac{2m}{\delta}(t - t_{i+1})\right)\right|^2 \\ &\leq \varphi_{\mathcal{A}(m)}\left(\frac{2m}{\delta}(t - t_i)\right) \mathbb{E}|X_{t_i}(\omega) - X_t(\omega)|^2 \\ &\quad + \varphi_{\mathcal{A}(m)}\left(\frac{2m}{\delta}(t - t_{i+1})\right) \mathbb{E}|X_{t_{i+1}}(\omega) - X_t(\omega)|^2 \\ &\leq \varphi_{\mathcal{A}(m)}\left(\frac{2m}{\delta}(t - t_i)\right) \mathcal{W}(X_t, \delta) \\ &\quad + \varphi_{\mathcal{A}(m)}\left(\frac{2m}{\delta}(t - t_{i+1})\right) \mathcal{W}(X_t, \delta) \\ &\leq \mathcal{W}(X_t, \delta), \end{aligned}$$

in view of the equation (7) and convexity of expectation.

If X_t is mean-square continuous, $\mathcal{W}(X_t, \delta) \rightarrow 0$ as $\delta = T/n \rightarrow 0$ as $n \rightarrow \infty$, which implies $\mathbb{E}[|\mathcal{S}_n(X_t, t) - X_t|^2] \rightarrow 0$ for each fixed t . Taking supremum in t yields the uniform statement $\sup_{t \in \mathcal{T}} \mathbb{E}[|\mathcal{S}_n(X_t, t) - X_t|^2] \leq \mathcal{W}(X_t, \delta) \rightarrow 0$, so the convergence is uniform in t as claimed. \square

Corollary 3.7 (Rate of convergence under Hölder condition). *Suppose there exist constants $C > 0$ and $0 < \alpha \leq 1$ such that*

$$\mathbb{E}[|X_t - X_s|^2] \leq C|t - s|^\alpha, \quad \forall s, t \in \mathcal{T}.$$

Then for every $t \in \mathcal{T}$,

$$\mathbb{E}[|\mathcal{S}_n(X_t, t) - X_t|^2] \leq C\delta^\alpha = C\left(\frac{T}{n}\right)^\alpha.$$

Consequently, $\mathcal{S}_n(X_t, t) \rightarrow X_t$ in mean square with rate $O(n^{-\alpha})$.

Proof. By definition of the modulus of continuity,

$$\mathcal{W}(X_t, \delta) = \sup_{|s-t| \leq \delta} \mathbb{E}[|X_t - X_s|^2].$$

Under the assumed Hölder condition,

$$\mathbb{E}[|X_t - X_s|^2] \leq C|t - s|^\alpha \leq C\delta^\alpha, \quad \text{whenever } |t - s| \leq \delta.$$

Taking supremum over all such s yields

$$\mathcal{W}(X_t, \delta) \leq C\delta^\alpha.$$

Applying Theorem 3.6, we obtain

$$\mathbb{E}[|\mathcal{S}_n(X_t, t) - X_t|^2] \leq \mathcal{W}(X_t, \delta) \leq C\delta^\alpha.$$

Since $\delta = \frac{T}{n}$, this becomes

$$\mathbb{E}[|\mathcal{S}_n(X_t, t) - X_t|^2] \leq C\left(\frac{T}{n}\right)^\alpha.$$

Thus,

$$\mathbb{E}[|\mathcal{S}_n(X_t, t) - X_t|^2] = O(n^{-\alpha}),$$

which completes the proof. \square

Now, we will explore the interpolating and convergence properties of our SINNOs defined in (3.1) in probability.

Theorem 3.8 (Uniform boundedness in probability). *Assume $(X_t)_{t \in \mathcal{T}}$ satisfies $\sup_{s \in \mathcal{T}} \mathbb{E}[|X_s|^2] < \infty$. Then the sequence $(\mathcal{S}_n(X_t, t))_{n \geq 1}$ is uniformly bounded in probability, i.e., for every $\varepsilon > 0$ there exists $M > 0$ such that*

$$\sup_{n \geq 1} \mathbb{P}(|\mathcal{S}_n(X_t, t)| \geq M) \leq \varepsilon.$$

Proof. By Theorem 3.2 there exists a constant $K > 0$ (independent of n) such that for all n and every fixed t , we have

$$\mathbb{E}[|\mathcal{S}_n(X_t, t)|^2] \leq K,$$

where $K = \mathcal{M}_0^2(\varphi_{\mathcal{A}(m)}) \sup_{s \in \mathcal{T}} \mathbb{E}[|X_s|^2]$. Using Markov (Chebyshev) inequality, we have

$$\mathbb{P}(|\mathcal{S}_n(X_t, t)| \geq M) \leq \frac{\mathbb{E}[|\mathcal{S}_n(X_t, t)|^2]}{M^2} \leq \frac{K}{M^2}.$$

Choosing M large enough ensures that the right-hand side is at most ε , proving uniform boundedness in probability. \square

Theorem 3.9 (Probability Convergence). *If $X_t(\omega) \in L^2(\Omega, \mathcal{F}, \mathbb{P})$. Then for every $i = 0, 1, \dots, n$, $\mathcal{S}_n(X_t, t_i)$ converges to $X_{t_i}(\omega)$ in probability as $n \rightarrow \infty$.*

Proof. For an arbitrary $\varepsilon > 0$, using the Chebyshev's inequality, we have

$$\mathbb{P}(|\mathcal{S}_n(X_t, t_i) - X_{t_i}(\omega)| \geq \varepsilon) \leq \frac{\mathbb{E}|\mathcal{S}_n(X_t, t_i) - X_{t_i}(\omega)|^2}{\varepsilon^2}.$$

In view of Theorem 3.3, we conclude that interpolation in probability holds good. \square

Theorem 3.10 (Strong Convergence). *If $X_t(\omega) \in L^2(\Omega, \mathcal{F}, \mathbb{P})$. Then $\mathcal{S}_n(X_t, t)$ converges to $X_t(\omega)$ almost surely.*

Proof. Define the event

$$A_n = \left\{ \omega \in \Omega : |\mathcal{S}_n(X_t, t) - X_t(\omega)| \geq \frac{1}{n} \right\}.$$

From probability convergence Theorem 3.9, we have

$$\sum_{n=1}^{\infty} \mathbb{P}(A_n) < \infty.$$

Applying the Borel-Cantelli Lemma, we conclude that

$$\mathbb{P}(A_n \text{ occurs infinitely often}) = 0.$$

Thus, for almost every ω , there exists λ such that for all $n \geq \lambda$,

$$|\mathcal{S}_n(X_t, t) - X_t(\omega)| < \frac{1}{n}.$$

This completes the proof as $n \rightarrow \infty$. □

Now, we investigate the path-wise approximation capabilities of our stochastic interpolation-NNOs (SINNOs).

For any fixed $\omega_i \in \Omega$, there exists a corresponding sample path $X_t(\omega_i)$ of the process $X_t(\omega)$. Depending on the properties of $X_t(\omega_i)$, we consider the following cases:

- V1. If $X_t(\omega_i) \in C(\mathcal{T})$, i.e., the sample path is continuous.
- V2. If $X_t(\omega_i) \in AC(\mathcal{T})$, i.e., the sample path is absolutely continuous.
- V3. If $X_t(\omega_i) \in L^p(\mathcal{T})$, i.e., the sample path belongs to the L^p space.

Under these conditions, the SINNOs introduced in (3.1) reduce to deterministic interpolation-NNOs :

$$\mathcal{S}_n(X_t(\omega_i), t) = \sum_{k=0}^n X_{t_k^{\omega_i}}(\omega_i) \varphi_{\mathcal{A}(m)} \left(\frac{2m}{\delta} (t - t_k^{\omega_i}) \right), \quad \omega_i \in \Omega, \quad t \in \mathcal{T}, \quad (8)$$

where the interpolation nodes $t_k^{\omega_i}$ are uniformly spaced time points given by $t_k^{\omega_i} = k\delta$, $k = 0, 1, \dots, n$, with $\delta = \frac{T}{n}$. Consequently, the results established in [14] remain valid for our SINNOs.

4 Numerical Validation

In this section, we provide numerical experiments and visual representations to confirm the effectiveness of the proposed stochastic interpolation neural network operators (SINNOs). The numerical validations are carried out using the MATLAB implementation presented below, which simulates the process $X_t(\omega)$ and evaluates the performance of SINNOs through interpolation and mean square approximation errors.

Algorithm 1 SINNOs Approximation Framework for a Stochastic Process $X_t(\omega)$

Given a second-order stochastic process $X_t(\omega) \in L^2(\Omega, \mathcal{F}, \mathbb{P})$, sigmoidal function $\eta \in \mathcal{A}(m)$, and its associated activation function $\varphi_{\mathcal{A}(m)}(t)$, the following steps construct and analyze the SINNOs approximation:

1. Fix the time horizon $[0, T]$, the number of realizations R , and a set of n -nodes.

2. For each realization $r = 1, 2, \dots, R$:

- (a) Simulate one realization $X_t^{(r)}(\omega)$ on a fine grid $\{t_i\}_{i=0}^n$.
- (b) Select a query point $t_q \in (0, T)$.

3. For n :

- (a) Define the interpolation nodes $t_k = kT/n$ with step size $\delta = T/n$.
- (b) Construct the SINNOs:

$$\mathcal{S}_n(X_t, t) = \sum_{k=0}^n X_{t_k}(\omega) \varphi_{\mathcal{A}(m)}\left(\frac{2m}{\delta}(t - t_k)\right).$$

- (c) Evaluate $\mathcal{S}_n(X_t, t)$ on both the interpolation nodes $\{t_k\}$ and the full interval $[0, T]$.
- (d) Compute the following mean square errors:

$$\text{MSE}_{\text{nodes}}(n) = \frac{1}{n} \sum_{k=0}^n \mathbb{E}[|X_{t_k} - \mathcal{S}_n(X_t, t_k)|^2],$$

$$\text{MSE}_{\text{query}}(n) = \mathbb{E}[|X_{t_q} - \mathcal{S}_n(X_t, t_q)|^2],$$

$$\text{MSE}_{\text{global}}(n) = \frac{1}{T} \int_0^T \mathbb{E}[|X_t - \mathcal{S}_n(X_t, t)|^2] dt.$$

4. Average the results over all realizations:

$$\overline{\text{MSE}}(n) = \frac{1}{R} \sum_{r=1}^R \text{MSE}^{(r)}(n).$$

5. Plot the approximated process and the corresponding error curves (node, query, and global MSE) with respect to n .

4.1 Simulation Model

Consider the Ornstein-Uhlenbeck (O-U) process $X_t(\omega)$ governed by the stochastic differential equation (SDE)

$$dX_t(\omega) = \theta(\mu - X_t(\omega)) dt + \sigma dW_t(\omega), \quad t \in [0, 10],$$

where $\theta > 0$ is the mean-reversion rate, μ is the long-term mean, $\sigma > 0$ is the volatility parameter, and $W_t(\omega)$ denotes the standard Wiener process (Brownian motion). For our simulation, we take the parameters

$$\theta = 0.5, \quad \mu = 0, \quad \sigma = 1, \quad X_0 = 0.$$

The stochastic process is simulated on a uniform fine-grid using the Euler-Maruyama discretization method. The ramp sigmoidal function

$$\eta_R(t) = \begin{cases} 0, & t \leq -\frac{1}{2}, \\ t + \frac{1}{2}, & -\frac{1}{2} < t < \frac{1}{2}, \\ 1, & t \geq \frac{1}{2}, \end{cases}$$

is used to construct the activation function $\phi_R(t)$, supported on $[-1, 1]$. The corresponding SINNO is implemented for both interpolation and approximation.

4.2 Numerical Setup

The MATLAB implementation is divided into three parts:

- (i) **Visualization:** Figure 4 illustrates the interpolation behavior of SINNOs for different number of interpolation nodes $n = 5, 10, 20, 50$. The O-U sample path is plotted alongside its corresponding SINNOs approximation.
- (ii) **Error Analysis:** Figures 5 and 6 display the mean square error (MSE) decay with respect to the number of interpolation nodes $n \in \{5, 10, \dots, 100\}$, evaluated both at nodes and globally across the interval.
- (iii) **Multi-realization Validation:** Figure 7 shows the comparison between the true O-U paths and the corresponding SINNOs approximation for three independent realizations at $n = 10$.

4.3 Results and Discussion

The numerical outcomes confirm the theoretical results obtained in the preceding sections:

1. SINNOs preserve the interpolation property at grid points, i.e., $\mathcal{S}_n(X_t, t_i) = X_{t_i}(\omega)$ almost surely.
2. The mean square error $\mathbb{E}|\mathcal{S}_n(X_t, t) - X_t(\omega)|^2$ decays uniformly as n increases, verifying the upper bound $\mathcal{O}(\mathcal{W}(X_t, \delta))$ derived in Theorem 3.6.
3. Empirically, both at node and global MSEs exhibit consistent convergence trends, reflecting the local averaging behaviour of the hat-type activation function.

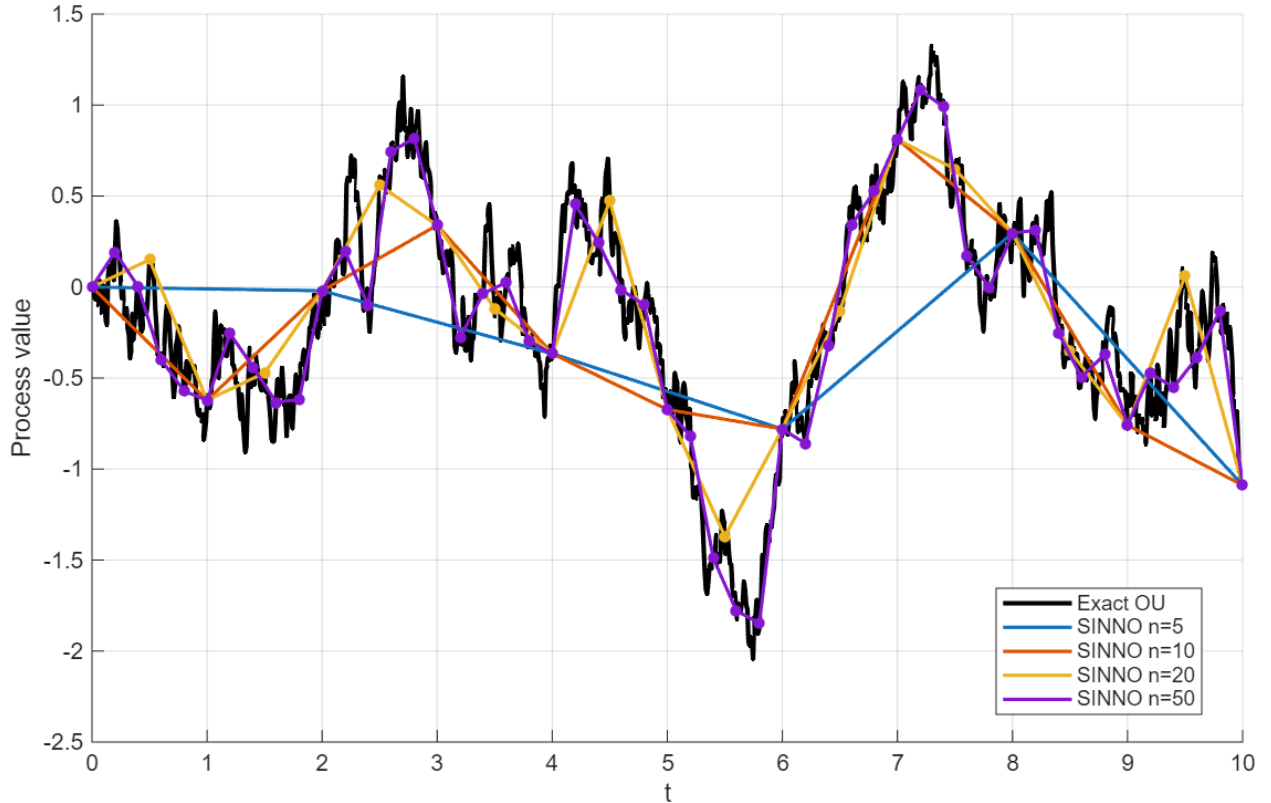


Figure 4: Approximation of the O-U process using SINNOs for $n = 5, 10, 20, 50$. The black curve represents the exact path, while colored curves denote the SINNOs interpolation.

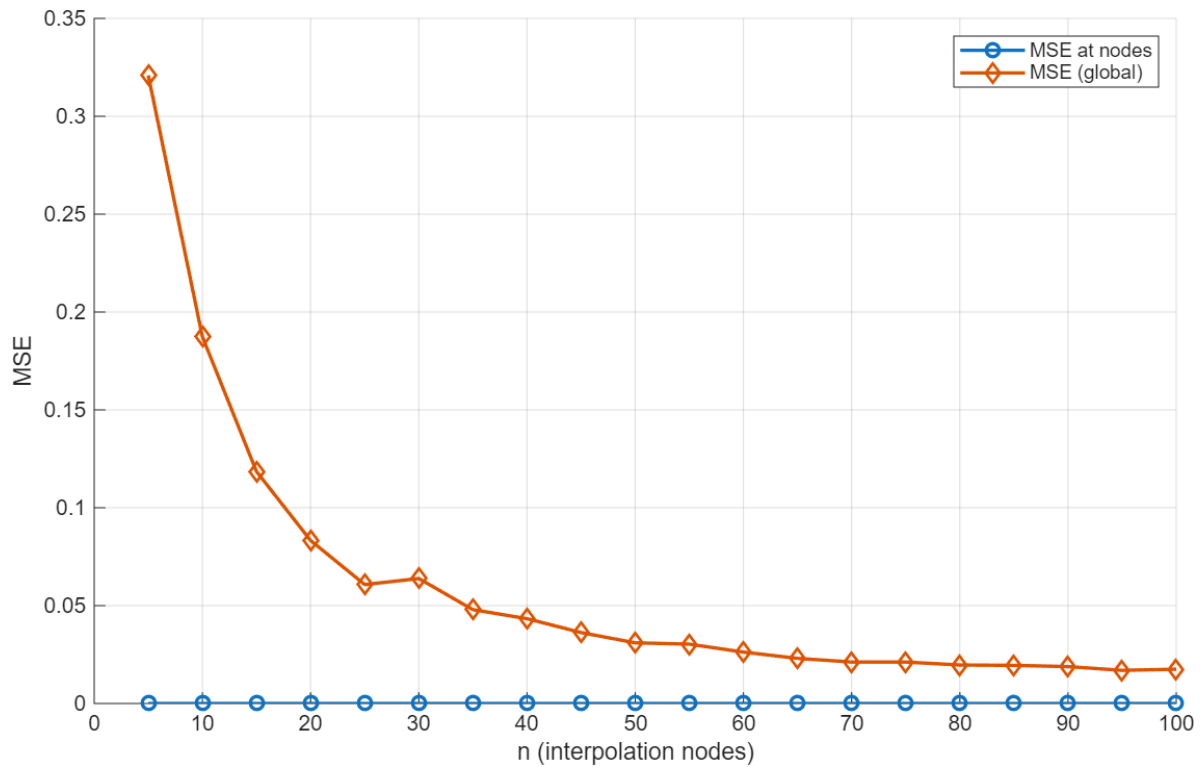


Figure 5: Uniform mean square error (MSE) vs. n for a single realization of the O-U process.

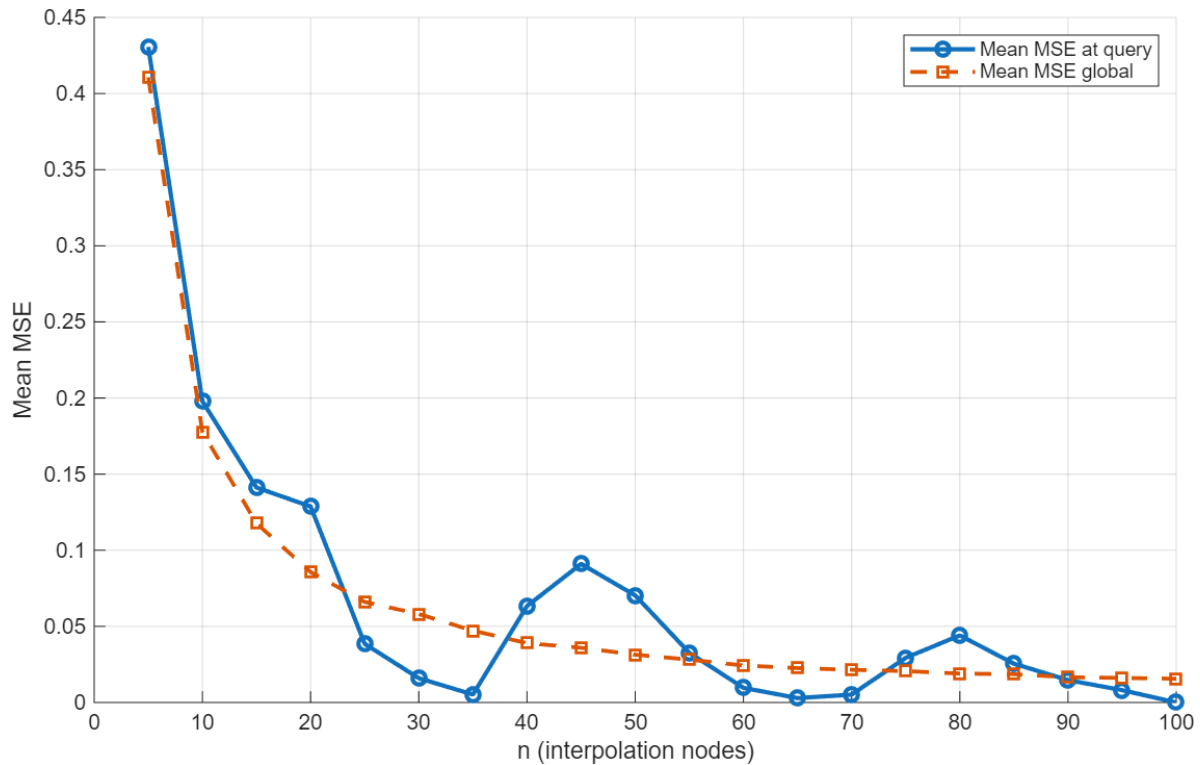


Figure 6: Monte Carlo mean MSE over three independent realizations of the O-U process, computed globally and at query points.

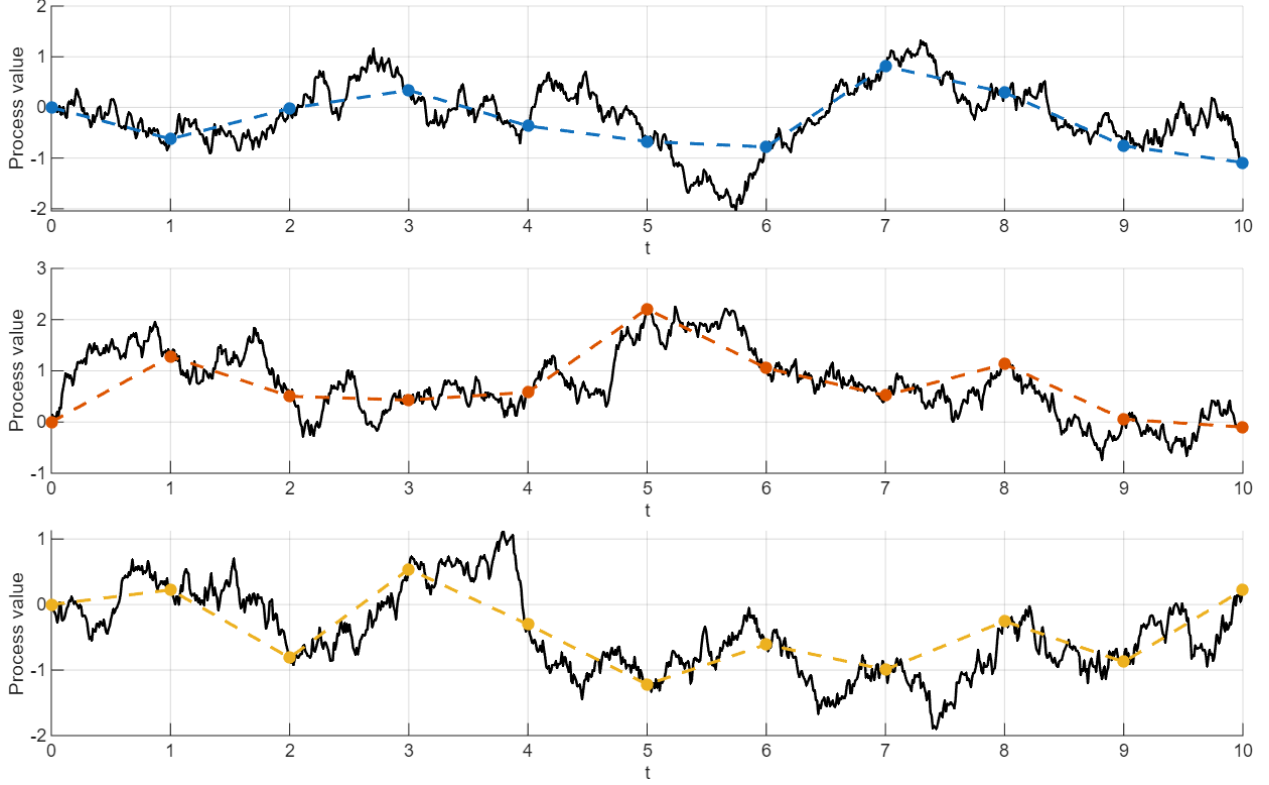


Figure 7: Three independent realizations of the O-U process (black) with corresponding SINNOs interpolation (colored dashed curves) for $n = 10$.

Figure 4 demonstrates that as n increases, SINNOs capture the stochastic dynamics of the O-U process more accurately, while Figures 5 and 6 quantitatively validate the theoretical rate of convergence. The three-realization comparison in Figure 7 further emphasizes the stability and robustness of the operator across stochastic paths.

4.4 Numerical Output and Observations

For a fixed query point $t_q = 3.70$, the numerical results averaged over three independent realizations of the Wiener process are summarized in Table 1. The table lists the mean interpolated value $\mathbb{E}[S_n(X_t, t_q)]$, the mean square error (MSE) at the query point, and its standard deviation (Std.) as the number of interpolation nodes n increases.

The above table clearly shows a monotonic decrease in the mean square error as n increases, indicating that the SINNOs approximation converges rapidly to the true process value at the query point. For $n \geq 30$, the MSE falls below 10^{-2} , and beyond $n = 65$ it becomes nearly negligible, consistent with the theoretical L^2 convergence rate.

4.5 Verification of the Interpolation Property

To further validate the interpolation capability of the SINNOs, Table 2 reports the node-wise results for three different realizations at $n = 10$. In all the cases, the absolute difference between the true values $X_{t_i}(\omega)$ and the interpolated ones $S_n(X_t, t_i)$ at the node points is zero, demonstrating that

$$S_n(X_t, t_i) = X_{t_i}(\omega) \text{ almost surely , } \quad \forall i = 0, 1, \dots, n.$$

For each realization, the operator perfectly reconstructs the stochastic sample at the interpolation nodes, while maintaining a bounded global error on the entire interval. The reduction in global MSE with increasing n reaffirms the stability and efficiency of the proposed SINNOs approximation for stochastic processes.

Overall, the numerical validations confirm that the SINNOs framework accurately reconstructs the stochastic trajectories while achieving consistent convergence in the mean square sense. This demonstrates the potential of SINNOs as reliable neural network operators for stochastic data approximation.

n	$\mathbb{E}[S_n]$	Mean(MSE $_q$)	Std(MSE $_q$)
5	-0.04119	4.3061×10^{-1}	5.239×10^{-1}
10	0.11046	1.9786×10^{-1}	2.364×10^{-1}
15	0.20949	1.4121×10^{-1}	1.044×10^{-1}
20	0.13182	1.2874×10^{-1}	9.941×10^{-2}
25	0.32901	3.8516×10^{-2}	3.867×10^{-2}
30	0.36355	1.5949×10^{-2}	1.567×10^{-2}
35	0.46211	5.2282×10^{-3}	5.070×10^{-3}
40	0.34450	6.3345×10^{-2}	6.482×10^{-2}
45	0.35213	9.1042×10^{-2}	1.276×10^{-1}
50	0.37575	7.0330×10^{-2}	4.840×10^{-2}
55	0.39755	3.2636×10^{-2}	4.054×10^{-3}
60	0.38865	9.6296×10^{-3}	1.540×10^{-2}
65	0.41149	2.8994×10^{-3}	2.604×10^{-3}
70	0.45298	5.1668×10^{-3}	3.876×10^{-3}
75	0.43877	2.9367×10^{-2}	2.271×10^{-2}
80	0.38331	4.4081×10^{-2}	3.907×10^{-2}
85	0.43879	2.5471×10^{-2}	2.111×10^{-2}
90	0.40156	1.4705×10^{-2}	2.138×10^{-2}
95	0.37897	8.0985×10^{-3}	8.352×10^{-3}
100	0.45883	5.2231×10^{-30}	7.827×10^{-30}

Table 1: Mean and mean square error (MSE) at the query point $t_q = 3.70$ averaged over 3 realizations.

Realization	MSE at nodes	MSE on fine grid
1	0.0000	1.8736×10^{-1}
2	0.0000	1.8052×10^{-1}
3	0.0000	1.6535×10^{-1}

Table 2: Interpolation property and global MSE for three realizations at $n = 10$.

4.6 Relation to diffusion and score-based generative models.

Recent advances in generative modeling have introduced diffusion models and score-based generative models, which learn stochastic dynamics through neural networks. In these approaches, a data sample is progressively perturbed by a forward diffusion process, and a neural network is trained to approximate the score function—the gradient of the log-density of the noisy data—so that the learned reverse diffusion (or stochastic differential equation) can generate new samples from the data distribution [37, 38, 39]. These models, therefore, learn a stochastic generative process by optimizing a neural network through score-matching or denoising objectives. In contrast, the present work introduces *stochastic interpolation neural network operators (SINNOs)*, which are analytic approximation operators rather than generative models. SINNOs employ fixed, compactly supported activation functions and stochastic coefficients derived directly from a given stochastic process, without a training stage or score-learning objective. Their purpose is to approximate or interpolate stochastic processes in the mean-square sense, with provable error bounds expressed via the modulus of continuity, rather than to synthesize new realizations. Conceptually, diffusion models and SINNOs share a common probabilistic and stochastic-process foundation—both rely on neural representations of stochastic behaviour—but serve complementary goals: diffusion models address data generation, whereas SINNOs focus on approximation theory and operator convergence. Establishing deeper theoretical connections between SINNO-type operators and score-based learning frameworks is an interesting direction for future research.

Remark 4.1. The approach for approximating the O-U process using SINNOs can be extended to other second-order stochastic processes. Since SINNOs inherently leverage the properties of smooth interpolation and the flexibility of neural network operators, they provide a robust framework for approximating a wide range of second-order stochastic processes. By adjusting the parameters of the neural network architecture and employing appropriate interpolation schemes, one can derive approximations for processes such as the Brownian motion, fractional Brownian motion, or more general Lévy processes, ensuring effective error bounds and rate of convergence for these processes as well.

5 Application

In this section, we present a real-data application of the proposed stochastic interpolation neural network operators (SINNOs) $\mathcal{S}_n(X_t, t)$. The objective is to evaluate their practical interpolation and prediction capability on time-dependent, stochastic-like real-world data.

For our study, we employ the **ramp sigmoidal function** $\eta_R(t) \in \mathcal{A}(\frac{1}{2})$, which generates the activation function

$$\varphi_R(t) = \eta_R\left(t + \frac{1}{2}\right) - \eta_R\left(t - \frac{1}{2}\right), \quad t \in \mathbb{R},$$

where $m = \frac{1}{2} > 0$ determines the support width of the activation function.

5.1 Dataset and Normalization

We apply $\mathcal{S}_n(X_t, t)$ to the daily COVID-19 case data from the **World Health Organization (WHO)** database (<https://data.who.int/dashboards/covid19/data?n=c>), stored in the file `WHO-COVID-19-global-daily-data.csv`. Each record consists of the pair

$$\{(t_k, X_{t_k}(\omega)) : t_k \in [0, T]\},$$

where $X_{t_k}(\omega)$ denotes the number of new cases reported on day t_k for a given country ω .

For this experiment, we fix $\omega^* = \text{India}$ and select the year 2020. The dataset consists of $n + 1$ observations

$$\{(t_k, X_{t_k}(\omega^*)) : k = 0, 1, \dots, n\},$$

where t_0 and t_n are the first and last observation dates. We apply a linear normalization of the time axis,

$$t_k \mapsto \frac{t_k - t_0}{t_n - t_0} \in [0, 1],$$

so that all computations and evaluations of $\mathcal{S}_n(X_t, t)$ are performed on the normalized interval $[0, 1]$. This transformation simplifies numerical implementation and aligns the dataset with the theoretical framework of SINNOs.

5.2 Implementation Details

Let n denote the number of interpolation nodes with spacing $\delta = 1/n$. For each n , the SINNOs approximation is computed as

$$\mathcal{S}_n(X_t, t) = \sum_{k=0}^n X_{t_k}(\omega^*) \varphi_R\left(\frac{2m}{\delta}(t - t_k)\right),$$

where φ_R is the activation function generated by η_R . The interpolant is evaluated on a grid $\{t_k\}_{k=1}^n$ to visualize the continuous reconstruction.

To assess accuracy, we compute the following numerical metrics:

$$\begin{aligned} \text{MSE}_{\text{nodes}} &= \frac{1}{n+1} \sum_{k=0}^n |X_{t_k}(\omega^*) - \mathcal{S}_n(X_t, t_k)|^2, \\ \text{MSE}_{\text{global}} &= \int_0^1 \mathbb{E}[|X_t(\omega^*) - \mathcal{S}_n(X_t, t)|^2] dt. \end{aligned}$$

Additionally, a hold-out validation is carried out by excluding the last $D = 14$ days of data and evaluating

$$\text{RMSE}_{\text{holdout}} = \sqrt{\frac{1}{D} \sum_{k=n-D+1}^n [X_{t_k}(\omega^*) - \mathcal{S}_n(X_t, t_k)]^2}.$$

All experiments are implemented in MATLAB using a vectorized realization of $\mathcal{S}_n(X_t, t)$ based on the ramp activation φ_R .

5.3 Numerical Results

For visualization, the case $n = 100$ was used, producing a smooth reconstruction $\mathcal{S}_n(X_t, t)$ that closely follows the actual daily case trajectory, as shown in Figure 8. The interpolated curve accurately captures oscillations in the COVID-19 time series while filtering out high-frequency noise.

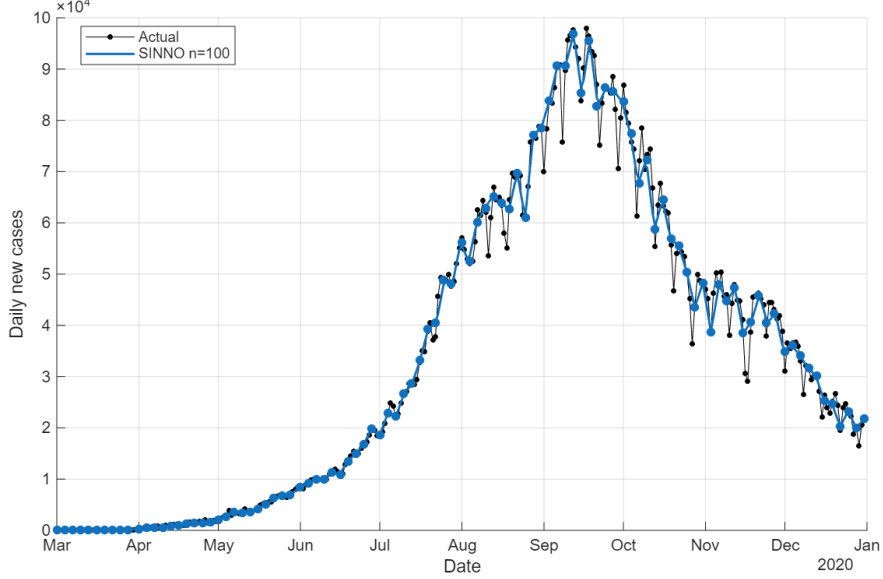


Figure 8: Prediction of daily COVID-19 cases in India using $\mathcal{S}_n(X_t, t)$ with the ramp activation φ_R for $n = 100$. The black curve shows actual data, and the blue curve shows the SINNOs reconstruction.

To investigate convergence, we vary n from 5 to 100 and evaluate both pointwise and global mean-square errors. Representative results are reported in Figure 9, showing a clear decay of the MSE with increasing n .

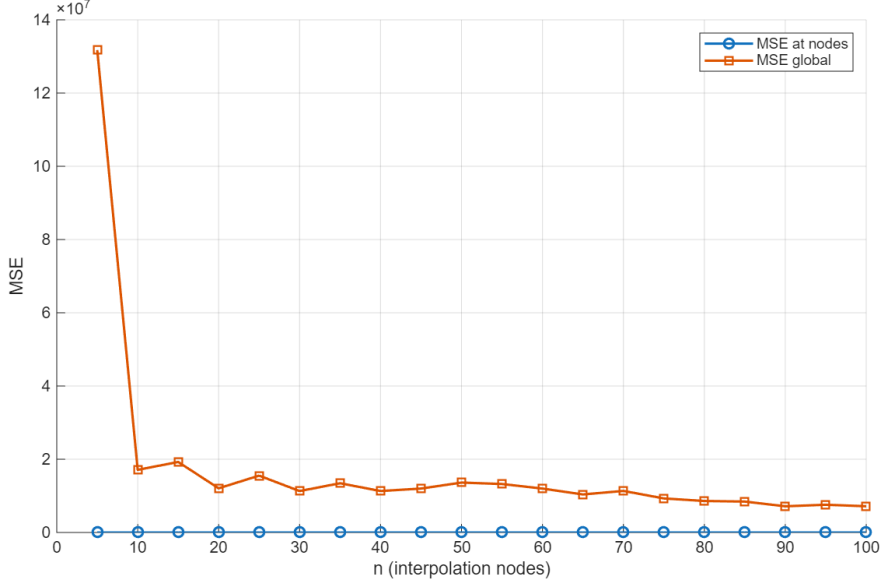


Figure 9: MSE decay of the SINNO approximation for COVID-19 daily cases in India (2020). Both node-wise and global errors decrease with increasing n , validating the convergence behaviour of the operator.

The hold-out evaluation on the last 14 days yields

$$\text{RMSE}_{\text{holdout}} = 2.0919 \times 10^4,$$

confirming that the proposed SINNOs generalizes well to unseen temporal samples and preserves stability in practical stochastic-like data approximation.

5.4 Discussion

The empirical study demonstrates that the proposed $\mathcal{S}_n(X_t, t)$ operator successfully interpolates stochastic-like temporal signals. The mean-square convergence in the stochastic sense,

$$\mathbb{E}|\mathcal{S}_n(X_t, t) - X_t(\omega)|^2 = \|\mathcal{S}_n(X_t, t) - X_t(\omega)\|_{L^2(\Omega)}^2 \longrightarrow 0, \quad \text{as } n \rightarrow \infty,$$

is consistent with the observed numerical decay of MSE. Hence, the SINNOs constructed with ramp activation not only preserve the theoretical convergence framework but also exhibit robustness and smoothness in real data reconstruction.

Overall, this experiment validates the effectiveness of SINNOs for data-driven stochastic approximation problems, such as modeling pandemic dynamics or other nonstationary time-series processes.

5.5 Multi-Country Extension

To further test the scalability and universality of the SINNOs framework, we extend the analysis to multiple countries, specifically India, the United States of America, China, and Brazil. For each country ω_i , the SINNOs approximation $\mathcal{S}_n(X_t^{(\omega_i)}, t)$ was computed using identical parameters ($m = 0.5$, $n = 100$), and the resulting reconstructions were plotted on a common time axis for visual comparison.

The SINNO plots revealed distinct epidemic dynamics across countries, yet all approximations maintained smooth transitions and local consistency with actual data trends. Furthermore, the 14-day hold-out RMSE remained within stable bounds for all four datasets, illustrating the robustness of the SINNOs approach in cross-regional epidemiological modeling.

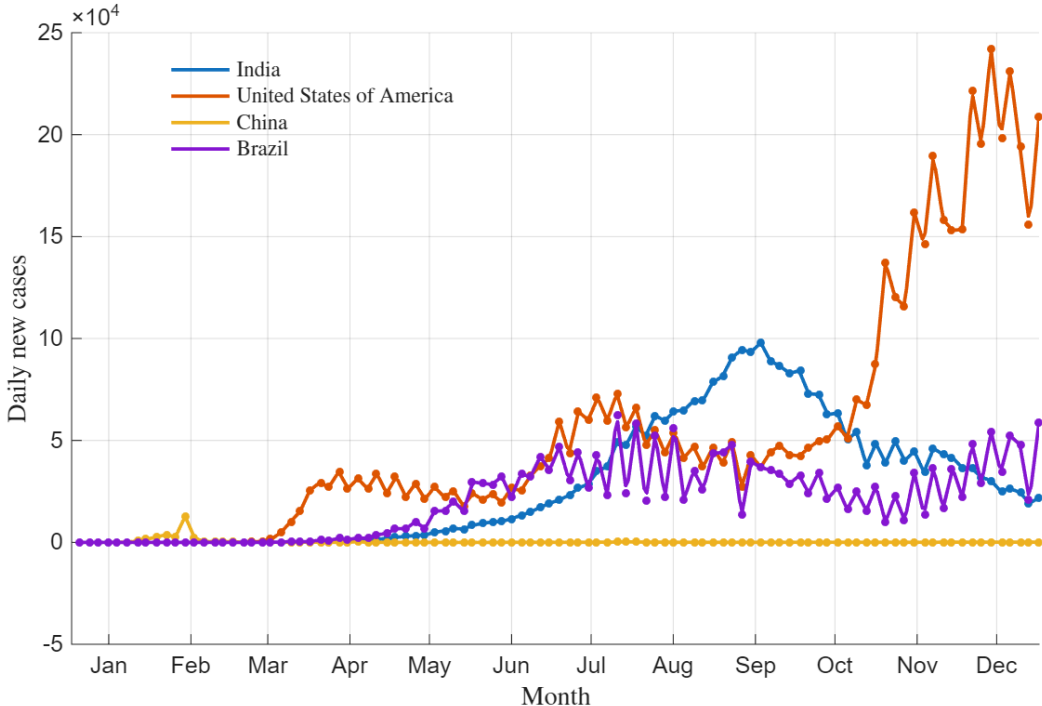


Figure 10: SINNOs predictions of daily COVID-19 cases for multiple countries (India, USA, China, Brazil). Each colored curve corresponds to $\mathcal{S}_n(X_t, t)$ with $n = 100$.

Country	RMSE _{holdout}
India	2.0919×10^4
United States of America	1.8672×10^5
China	8.7668×10^1
Brazil	4.3336×10^4

Table 3: Hold-out RMSE comparison across multiple countries for the SINNOs interpolation of daily COVID-19 cases (year 2020). Each value represents the root-mean-square error computed over the last 14 days of each country’s dataset.

The numerical comparison highlights that the SINNOs model adapts well across diverse temporal profiles. While the United States exhibits higher error due to large-scale fluctuations in daily case counts, China’s very low RMSE reflects a more stationary regime with fewer abrupt changes. India and Brazil show intermediate error magnitudes, confirming that the proposed SINNOs maintains consistent predictive stability across heterogeneous epidemiological patterns.

This demonstrates that the SINNOs framework, originally designed for stochastic interpolation in $L^2(\Omega, \mathcal{F}, \mathbb{P})$, can generalize to large-scale, heterogeneous datasets across regions. Such adaptability highlights the potential of SINNOs-type neural operators for practical applications in global data modeling, epidemiological forecasting, and other temporal stochastic systems.

6 Conclusion

This work introduced stochastic interpolation neural network operators (SINNOs) for approximating the Ornstein-Uhlenbeck (O-U) process using a ramp activation function. Theoretical estimates and mean-square error plots (Figures 5-6) confirm convergence as the number of interpolation points increases, while visual comparisons (Figures 4-7) illustrate the accuracy of the approximation relative to the O-U process. The SINNOs framework was further applied to real-world data, where it successfully reconstructed daily COVID-19 case trajectories for India and, subsequently, for multiple countries, including the United States, China, and Brazil. The operators effectively captured heterogeneous temporal dynamics and preserved smoothness across varying data scales (Figure 10). Quantitative evaluations (Table 3) reported low hold-out RMSE values, particularly for stable regions such as China, confirming consistent generalization performance.

Overall, these results show that SINNOs are both theoretically sound and empirically robust for modeling stochastic-like signals and time-series data. Future directions include extending SINNOs to higher-dimensional stochastic processes, exploring alternative activation functions, applying the operators in finance and physics, and integrating SINNOs with deep neural architectures to further enhance accuracy and stability.

Declaration of competing interest

The authors declare that they have no competing financial interests or personal relationships that could influence the reported work in this paper.

References

- [1] George Cybenko. Approximation by superpositions of a sigmoidal function. *Math. Control Signals Syst.*, 2(4):303–314, 1989.
- [2] Ken Ichi Funahashi. On the approximate realization of continuous mappings by neural networks. *Neural Netw.*, 2(3):183–192, 1989.
- [3] Pierre Cardaliaguet and Guillaume Euvrard. Approximation of a function and its derivative with a neural network. *Neural Netw.*, 5(2):207–220, 1992.
- [4] George A Anastassiou. Rate of convergence of some neural network operators to the unit-univariate case. *J. Math. Anal. Appl.*, 212(1):237–262, 1997.
- [5] George A Anastassiou. Rate of convergence of some multivariate neural network operators to the unit. *Comput. Math. Appl.*, 40(1):1–19, 2000.
- [6] George A Anastassiou. Multivariate sigmoidal neural network approximation. *Neural Netw.*, 24(4):378–386, 2011.
- [7] George A Anastassiou. Univariate sigmoidal neural network quantitative approximation. *Intelligent Systems: Approximation by Artificial Neural Networks*, pages 1–32, 2011.

[8] George A Anastassiou. Univariate hyperbolic tangent neural network approximation. *Math. Comput. Model.*, 53(5-6):1111–1132, 2011.

[9] George A. Anastassiou. Multivariate hyperbolic tangent neural network approximation. *Comput. Math. Appl.*, 61(4):809–821, 2011.

[10] George A Anastassiou. Fractional approximation by normalized bell and squashing type neural network operators. *New Math. Nat. Comput.*, 9(01):43–63, 2013.

[11] George A Anastassiou. Rate of convergence of some multivariate neural network operators to the unit, revisited. *J. Comput. Anal. Appl.*, 15(1):1300–1309, 2013.

[12] Danilo Costarelli. Interpolation by neural network operators activated by ramp functions. *J. Math. Anal. Appl.*, 419(1):574–582, 2014.

[13] Danilo Costarelli. Neural network operators: constructive interpolation of multivariate functions. *Neural Netw.*, 67:28–36, 2015.

[14] Yunyou Qian and Dansheng Yu. Rates of approximation by neural network interpolation operators. *Appl. Math. Comput.*, 418:126781, 2022.

[15] Guoshun Wang, Dansheng Yu, and Lingmin Guan. Neural network interpolation operators of multivariate functions. *J. Comput. Appl. Math.*, 431:115266, 2023.

[16] Fesal Baxhaku, Artan Berisha, Purshottam Narain Agrawal, and Behar Baxhaku. Multivariate neural network operators activated by smooth ramp functions. *Expert Syst. Appl.*, 269:126119, 2025.

[17] Purshottam N Agrawal and Behar Baxhaku. Neural network interpolation operators based on lagrange polynomials. *Rev. R. Acad. Cienc. Exactas Fís. Nat. Ser. A Mat.*, 119(1):11, 2025.

[18] Manju Sharma and Uday Singh. Approximation by a neural network interpolation operator for irregular grid points. *J. Nonlinear Convex Anal.*, 24(9):1919–1928, 2023.

[19] Danilo Costarelli, Michele Piconi, Manju Sharma, and Uday Singh. Higher order convergence of a multivariate neural network interpolation operator for irregular grid. *Results Math.*, 80(6):1–17, 2025.

[20] Manju Sharma and Uday Singh. Fractional neural network interpolation operator for irregular grid points. In *ISAAC Congr.*, pages 359–371. Springer, 2023.

[21] Ugur Kadak. Multivariate fuzzy neural network interpolation operators and applications to image processing. *Expert Syst. Appl.*, 206:117771, 2022.

[22] Shunichi Amari, Koji Kurata, and Hiroshi Nagaoka. Information geometry of boltzmann machines. *IEEE Trans. Neural Netw.*, 3(2):260–271, 1992.

[23] Jieyu Zhao and John Shawe-Taylor. A recurrent network with stochastic weights. In *Proceedings of International Conference on Neural Networks (ICNN'96)*, volume 2, pages 1302–1307. IEEE, 1996.

[24] Marcello R Belli, Massimo Conti, Paolo Crippa, and Claudio Turchetti. Artificial neural networks as approximators of stochastic processes. *Neural Netw.*, 12(4-5):647–658, 1999.

[25] Yuly Makovoz. Random approximants and neural networks. *J. Approx. Theory*, 85(1):98–109, 1996.

[26] George A Anastassiou and Dimitra Kouloumpou. Brownian motion approximation by neural networks. *Commun. Optim. Theory*, 2022.

[27] George A Anastassiou and Dimitra Kouloumpou. Brownian motion approximation by parametrized and deformed neural networks. *Revista de la Real Academia de Ciencias Exactas, Físicas y Naturales. Serie A. Matemáticas*, 118(1):14, 2024.

[28] George A Anastassiou and Dimitra Kouloumpou. Approximation of brownian motion on simple graphs. *Mathematics*, 11(20):4329, 2023.

[29] George A Anastassiou and Dimitra Kouloumpou. Neural network approximation for time splitting random functions. *Mathematics*, 11(9):2183, 2023.

[30] Emanuele Ledda, Giorgio Fumera, and Fabio Roli. Dropout injection at test time for post hoc uncertainty quantification in neural networks. *Inf. Sci.*, 645:119356, 2023.

[31] Ugur Kadak. Durrmeyer deep neural networks: Bridging deep learning and dynamic brain functional connectivity. *Inf. Sci.*, page 122623, 2025.

[32] Jie Ren, Qimin Zhang, Feilong Cao, Chunmei Ding, and Li Wang. Modeling a stochastic age-structured capital system with poisson jumps using neural networks. *Inf. Sci.*, 516:254–265, 2020.

- [33] Changqing Yuan, Yongfang Xie, Shiwen Xie, and Zhaohui Tang. Interval type-2 fuzzy stochastic configuration networks for soft sensor modeling of industrial processes. *Inf. Sci.*, 679:121073, 2024.
- [34] Jérémie Cabessa and Yann Strozecki. Refined kolmogorov complexity of analog, evolving and stochastic recurrent neural networks. *Inf. Sci.*, 711:122104, 2025.
- [35] JL Doob. Stochastic processes. wiley classics library, 1990.
- [36] Guoshun Wang, Dansheng Yu, and Lingmin Guan. Neural network interpolation operators of multivariate functions. *J. Comput. Appl. Math.*, 431:115266, 2023.
- [37] Jonathan Ho, Ajay Jain, and Pieter Abbeel. Denoising diffusion probabilistic models. In *Advances in Neural Information Processing Systems (NeurIPS)*, pages 6840–6851, 2020.
- [38] Yang Song, Jascha Sohl-Dickstein, Diederik P Kingma, Abhishek Kumar, Stefano Ermon, and Ben Poole. Score-based generative modeling through stochastic differential equations. In *International Conference on Learning Representations (ICLR)*, 2021.
- [39] Ling Yang, Zhiyong Zhang, Yifei Song, Zhihao Hong, Yong Xu, Meng Wang, Xiaohu Hong, Zongben Xu, and Dacheng Tao. Diffusion models: A comprehensive survey of methods and applications. *ACM Computing Surveys*, pages 1–39, 2023.